

Superconducting Neutron Detectors and Their Application to Imaging

Takekazu ISHIDA^{†a)}, *Nonmember*

SUMMARY Superconducting detectors have been shown to be superior to other techniques in some applications. However, superconducting devices have not been used for detecting neutrons often in the past decades. We have been developing various superconducting neutron detectors. In this paper, we review our attempts to measure neutrons using superconducting stripline detectors with DC bias currents. These include attempts with a MgB₂-based detector and a Nb-based detector with a ¹⁰B converter. **key words:** *superconducting detector, neutron, kinetic inductance, delay-line imaging*

1. Introduction

Historically, nuclear research reactors were needed to supply continuous neutron beams for various types of research. In recent years, high-intensity pulsed neutron sources have come online at large-scale facilities in the several countries. However conventional neutron detectors cannot exploit the full potential of such facilities. We expect that superconducting neutron detectors will be useful for conducting transmission imaging. In the coming years further progress is expected in high-end neutron facilities across the globe, hence we have been developing superconducting neutron detectors with the goal of achieving superior performance to conventional neutron detectors. We developed a current-biased transition edge detector (CB-TED) using MgB₂ and succeeded in observing neutrons. More recently, we developed a delay-line current-biased kinetic inductance detector (CB-KID) with a ¹⁰B conversion layer for neutrons which utilizes ¹⁰B(n,⁴He)⁷Li reactions. The local deposition of energy by light-ions released from the reactions creates mesoscopic hot-spots, from which pulsed electromagnetic waves propagate along the superconducting stripline with matched impedance and low attenuation towards the end electrodes. By measuring the four arrival timestamps of signals at the electrodes, we can evaluate the hotspot (*x, y*) coordinate using a delay-line technique (see Fig. 4, below).

If it is possible to measure transmission neutron images with micrometer resolution, we expect that a scientific field will develop based around the observation of light elements on the micron scale. Potential applications include studying the hydrogen embrittlement of metals, observing water in plant root and soil systems, and observing electro-chemical

fields in lithium batteries.

In this paper, we describe the history behind the development of superconducting detectors, our attempts to develop superconducting neutron detectors, and recent results on transmission neutron imaging using a current-biased kinetic inductance detector.

2. Brief History of Superconducting Detectors

The advantages of superconducting detectors are recognized as (1) high sensitivity, (2) high-speed operation, (3) high resolution, and (4) small energy dissipation. It is often impossible to achieve the level of performance of superconducting sensors using conventional techniques.

Previously developed superconducting detectors include (A) a superconducting tunnel junction (STJ) detector [1]–[3], (B) a superconducting transition edge sensor (TES) [4], [5], (C) a superconducting nanowire single photon detector (SNSPD) [6], [7], and (D) a microwave kinetic inductance detector (MKID) [8]. The merits of these superconducting detectors have been investigated in comparison to other techniques.

Although it has been very attractive to know that various superconducting detectors have been very successful to measure various external excitations, we notice that the superconducting detector has not frequently been applied to measure neutrons. In the next section, we mention the applications of the superconducting detectors to measure neutrons. It is often pointed out that a difficulty of superconducting devices is the need to cool the sensors down to cryogenic temperatures. This issue has to be overcome to pursue the advantages of superconducting devices. We note that CB-KID has the merits of low self-heating and heat load.

3. Superconducting Neutron Detectors

The neutron is known to have a nearly identical mass to the proton (1.008665 u, where u is the atomic mass unit), a spin of 1/2, and a magnetic moment of -1.9132 erg/G. However, as neutrons have neutral charge, we cannot utilize the Coulomb interaction to detect them. Existing neutron detectors utilize various useful nuclear reactions to convert neutrons and enable detection. For example, ¹⁰BF₃ gas counters use the ¹⁰B(n, α)⁷Li reaction, and ³He counters use the ³He(n,p)³T reaction. Gas counters need to be a certain size to operate, and cannot be as small as the millimeter scale. Moreover, the dead time of ¹⁰BF₃ counters

Manuscript received August 26, 2019.

Manuscript revised November 21, 2019.

[†]The author is with Division of Quantum and Radiation Engineering, Graduate School of Engineering, Osaka Prefecture University, Sakai-shi, 599–8570 Japan.

a) E-mail: ishida@center.osakafu-u.ac.jp

DOI: 10.1587/transele.2019SEI0002

is $7 \mu\text{s}$, and that of ^3He is $8 \mu\text{s}$ [9], so these systems are not suitable for measuring high intensity neutron beams. In addition, ^6Li scintillation counters have a decay time of $7 \mu\text{s}$ [10] and micro-channel plate detectors have a dead time of $100 \mu\text{s}$ [11]. However, they require additional space to install optical readout apparatus and a CMOS readout device. Therefore, it does not seem possible to install these detectors in a multi-stacked configuration. We consider that further high-speed neutron detectors would be desirable in view of the recent progress of strong pulsed neutrons.

Contrary to X-rays, neutron beams are suitable for probing the distribution of light elements such as hydrogen, lithium, carbon, and oxygen. However, it is not easy to make observations on the micrometer-scale due to the difficulty of realizing high-resolution neutron optics. There would be a large impact if a neutron microscope could resolve images on the micrometer resolution, as traditional optical and electron microscopes are able to do.

Superconducting detectors have advantages in observing various external stimuli (X-ray, photon, gamma-ray, nuclear particles, etc.), however there have only been limited applications for observing neutrons. The Akimitsu Group discovered superconductivity in magnesium diboride (MgB_2) at $T_c = 39 \text{ K}$ [9]. After this discovery, we proposed the idea of using this material in a neutron detector by exploiting the $^{10}\text{B}(n,\alpha)^7\text{Li}$ nuclear reaction [13].

We began developing an MgB_2 neutron detector in 2001, and successfully observed neutrons using MgB_2 wire for the first time in 2008 [14]. Stable boron-10 enriched Mg^{10}B_2 has a huge cross-section for the $^{10}\text{B} + n \rightarrow \alpha + ^7\text{Li}$ nuclear reaction (3835 barns for thermal neutrons of 25 meV). The nuclear reaction has a branching ratio of 94% for emitting a 0.84-MeV lithium particle and a 1.47-MeV alpha particle. This detector was called the current-biased transition edge detector (CB-TED), and it was used first for the observation of cold neutrons from the research reactor JRR-3M at temperatures in the vicinity of a critical temperature (see Fig. 1) [14]. This detector utilizes a transient change in the bias current via a mutual inductor as shown in schematic diagram of Fig. 1.

When developing the MgB_2 detector, we needed to achieve an accuracy of within $0.1 \mu\text{m}$ for drawing connections with electron beam lithography. This was achieved by a dry etching the MgB_2 wire using electron cyclotron resonance etching. Subsequently a reactive etching method (RIE) using $\text{Br}_2\text{-N}_2$ gas was developed for etching the MgB_2 nanowire [15]. Molecular beam epitaxy (MBE) deposition of the MgB_2 film was developed for using the lift-off method for the fine fabrication of the MgB_2 devices [16]. These techniques will enable further development of the MgB_2 detector without using a dry etching in fabrication. However, we recognized that it is difficult with the MgB_2 detector to achieve a bias temperature of the detector within a certain narrow temperature regime if multiplexing detectors for imaging.

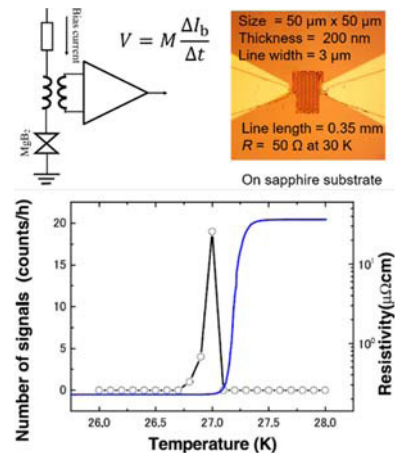


Fig. 1 Photograph and schematic diagram of the MgB_2 detector and. The MgB_2 detector was biased by $150 \mu\text{A}$ DC current. Output signals via mutual inductor were observed by a 5 GHz digital oscilloscope through an ultra-low-noise amplifier. The number of neutron events detected by the MgB_2 detector is shown as a function of temperature. The resistivity of the MgB_2 wire is also shown as a function of temperature for comparison [11].

4. Current-Biased Kinetic Inductance Detector

As a next advancement for superconducting neutron detectors, we proposed the idea of a Nb stripline detector utilizing a ^{10}B neutron conversion layer for achieving high spatial resolution imaging [17]–[20]. The detector was called the current-biased kinetic inductance detector (CB-KID), as it utilizes local changes in the kinetic inductance of Nb nanowires. Although a current-biased transition edge detector utilizes a rapid change in a resistance of MgB_2 wire, CB-KID is able to use a wide temperature regime for operation. In addition, CB-KID differs from other superconducting detectors because it utilizes a local response of the detector. We successfully gave a theoretical model utilizing a local electrodynamic response in a hot spot of the superconducting meanderline [21], [22]. The MKID, for example, probes a change of the kinetic inductance of the whole meanderline through a change in the resonance frequency of the LC tank circuit. On the contrary, CB-KID yields a signal due to an electrodynamic response of a mesoscopic hot spot as a time-dependent change of the local kinetic inductance. We consider that this method of operation is in contrast with other sorts of kinetic inductance detector. CB-KID requires a bias current across the superconducting nanowire to generate a pair of signals, but the bias current can be much smaller than the critical current in marked contrast with SNSPD. We employed a delay-line technique to image the distribution of mesoscopic hot spots through the timestamps of the signal arrivals at the electrodes. Since the nanowire and the Nb ground plane can form a coplanar stripline and act as a waveguide for the travelling electromagnetic waves, it is suitable for utilizing the delay-line technique, which requires long-distance signal transmissions with small dissipation losses.

A typical signal amplitude was $\sim 50 \text{ mV}$ and a pulse

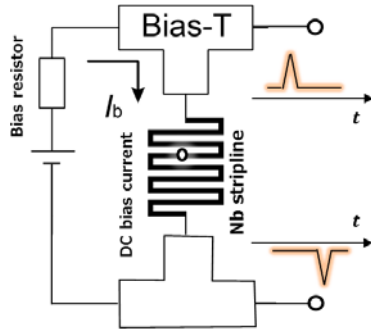


Fig. 2 The CB-KID meanderline under the DC bias current gives rise to a pair of positive and negative signals when a hot spot (mesoscopic excitation) appears by an external stimulus. This is caused by an instantaneous change in the number of Cooper pairs as $d(\Delta L_K)/dt$. Generated signals propagate along the stripline at a constant velocity towards the electrodes as electromagnetic waves.

width was ~ 30 ns while the signal was amplified by an amplifier of gain 200 [20]. We empirically explain the principle by which signals are generated from a CB-KID composed of Nb nanowire. The kinetic inductance of a superconductor can be expressed as $L_K = m_s \ell / n_s q_s S$, where m_s is the mass of a superconducting electron, n_s is the density of superconducting electrons, q_s is the charge of a superconducting electron, ℓ is the length of superconducting wire, S is the cross-section of the superconducting wire. One can enhance the kinetic inductance L_K by reducing the cross-section of the wire relative to the magnetic inductance L_M . In Fig. 2, we show a schematic diagram explaining the operation of CB-KID. The DC bias current I_b is fed through a bias resistor from a voltage source. The ^{10}B conversion layer of neutrons, which is placed on top of the double meanderlines, produces a 0.84-MeV ^7Li particle and a 1.147-MeV ^4He particle by the $^{10}\text{B}(n,^4\text{He})^7\text{Li}$ nuclear reaction. A small fraction of kinetic energy (~ 20 keV) of the particle [23] is deposited in the Nb wire causing a partial breaking of the Cooper pairs in a restricted portion $\Delta\ell$ of the Nb nanowire. This yields an instant change in a kinetic inductance ΔL_K and a resultant voltage signal as $V(t) = I_b d(\Delta L_K)/dt$. Note that not only ΔL_K , but also $d(\Delta L_K)/dt$ contribute to the signal amplitude. Since the Cooper pairs are broken on a very short timescale, the signal amplitude can be a measurable amplitude even if the kinetic inductance ΔL_K involved is not so large. We estimated an output (~ 0.6 mV) from CB-KID using the empirical relation.

Our original idea was to divide the meanderline with several electrodes to obtain several pixels (see Fig. 3). However, branching of the meanderline was the origin of signal reflections and distortions. In addition, it is not so easy to place a number of electrode taps in the meanderline and achieve a high number of pixels due to limitations of the readout circuits and fabrication techniques. Instead, we consider the idea of a delay-line technique for fulfilling multiplexing. We need a good transmission line for a pair of pulsed signals to ensure an operation of the delay-line method. Theoretical analysis of the CB-KID detector is given by Koyama and Ishida [21]. They showed that

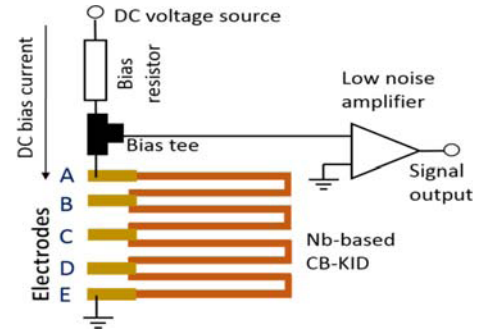


Fig. 3 Schematic diagram of the CB-KID system with multiple electrode taps dividing the stripline into different pixels. The intention was to develop a multi-pixel imaging device. However, branching of the meanderline was the source of signal distortions.

the electromagnetic wave propagates along the stripline as a Swihart pulse. They also derived a theoretical prediction of the pulse shape in terms of the time-dependent Ginzburg-Landau theory [22].

5. Imaging with the Delay-Line CB-KID Method

The delay-line CB-KID has an orthogonal stack of an X meanderline, a Y meanderline together, a ground plane, and a ^{10}B neutron-conversion layer. Both X and Y meanderlines give a pair of electromagnetic signals. The four signals are used to identify the position of mesoscopic hot spots and compose an image.

Only four readouts are necessary to be connected from the cryogenic detector to room-temperature electronics, and hence the refrigeration load is fairly small due to small heat conduction to the cryogenic detector. The CB-KID operates at the zero-resistance state under the DC bias current, as the Joule heating is negligibly small. These conditions are advantageous for mounting the superconducting detector to the cryostat.

Transmission imaging with neutron beams can be obtained as an intensity histogram of neutrons after passing through the sample. For example, CB-KID consists of X and Y superconducting Nb striplines with $1\text{-}\mu\text{m}$ width that are folded within an $h = 10.5$ mm segment with a spacing of $1\ \mu\text{m}$. Thus the repetition period is $p = 2\ \mu\text{m}$ and the total meanderline length extends to $\ell = 52.5$ m. Seven layers were stacked sequentially from bottom to top as follows: 1) a silicon substrate with $625\text{-}\mu\text{m}$ thickness, 2) a 300-nm -thick SiO_2 layer, 3) a superconducting Nb ground plane with 300-nm thickness, 4) an insulating SiO_2 layer with 250-nm thickness, 5) a superconducting 40-nm -thick Nb Y meanderline, 6) an insulating SiO_2 layer with 300-nm thickness, 7) a superconducting 40-nm -thick Nb X meanderline, 8) an insulating SiO_2 layer with 250-nm thickness, and 9) an enriched- ^{10}B neutron-capture layer with 300-nm thickness. Finally, CB-KID can be fabricated as a single chip on the silicon substrate.

The nuclear reaction $^{10}\text{B}(n,^4\text{He})^7\text{Li}$ mainly emits a 0.84-MeV ^7Li ion and a 1.47-MeV ^4He ion. The delay-

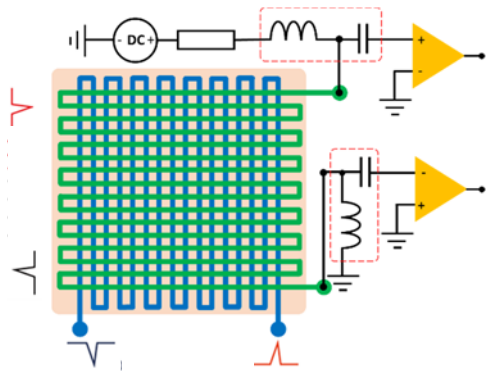


Fig. 4 Delay-line CB-KID with a ^{10}B conversion layer includes X and Y meanderlines. Energy dissipation by a charged particle creates mesoscopic hot spots in each meanderline, and subsequently generates pairs of electromagnetic waves. Propagation of the electromagnetic waves can be detected at the electrodes. The arrival timestamps are essential for identifying the position (x, y) of the hot spot and drawing the image.

line CB-KID can image the distribution of hot spots created within the detector. A pair of voltage pulses with opposite polarities originate at a hot spot on the meander line and propagate as electromagnetic waves towards both ends along the Nb meander line. We can identify the quartet signals originating from a single event, although several signals are simultaneously present on the meanderlines [20]. Since detection events of radiations can be stored as multiple travelling waves in a long stripline, the hit-count rate can be as high as 10^6 cps. In other words, CB-KID has a high multi-hit tolerance up to the temporal resolution limit to discriminate the signals from each other. The neutron incident position (X, Y) can be determined as $X = (t_{\text{Ch4}} - t_{\text{Ch3}})v_x p/2h$ and $Y = (t_{\text{Ch2}} - t_{\text{Ch1}})v_y p/2h$, where h is the length of each segment of the meander line, p is a repetition pitch for the meander line, t_{Ch1} , t_{Ch2} , t_{Ch3} , and t_{Ch4} are the corresponding time stamps of the signals received at the four channels of the Kalliope-DC circuit, where Ch3 and Ch4 are the ends of the X meanderline and Ch1 and Ch2 are the ends of the Y meanderline. By accumulating the hot spot locations, we obtain a neutron transmission image of any test sample by means of the delay-line CB-KID technique.

We conducted neutron beam irradiations of CB-KID to investigate a spatial resolution using a test absorber of ^{10}B dots at beam line BL10 of the Materials and Life Science Experimental Facility (MLF) at J-PARC. To evaluate the spatial resolution of CB-KID imaging experimentally, we conducted a neutron-imaging demonstration by using a well-shaped neutron absorber as a test pattern. The test absorber comprised a $50\text{-}\mu\text{m}$ -thick stainless-steel mesh ($15\text{ mm} \times 15\text{ mm}$ in size), wherein $100\text{ }\mu\text{m} \times 100\text{ }\mu\text{m}$ square holes were set in a square lattice (lattice constant $250\text{ }\mu\text{m}$). Each hole was filled by fine ^{10}B particles. In Fig. 5, we show a neutron-radiography image of the ^{10}B dots array, which matches the photo image of the test pattern. Measurements were performed at $T = 4.15\text{ K}$ with $I_x = 0.16\text{ mA}$ and $I_y = 0.48\text{ mA}$ for 30.4 h with an incident neutron wavelength λ ranging from 0.05 nm to 1.13 nm.

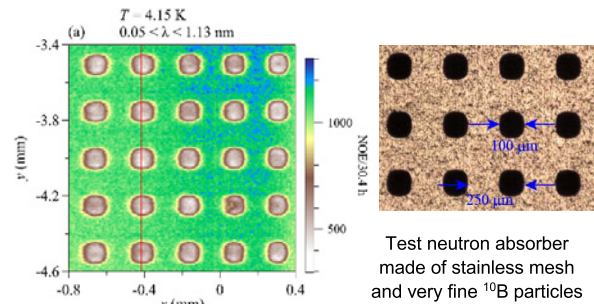


Fig. 5 Neutron transmission image of an array of ^{10}B dots using pulsed neutrons of wave lengths from 0.05 nm to 1.13 nm at J-PARC. Test sample was made using ^{10}B fine particles filled into holes in a $50\text{-}\mu\text{m}$ thick stainless-steel mesh. The ^{10}B dots are clearly seen in the transmission image [20].

We reconstructed a neutron image from the collected signal detecting timestamps in Ch1, Ch2, Ch3, and Ch4. The color scale indicates the number of events over 30.4 h. The hole size and repetition period were estimated from the neutron imaging as $106\text{ }\mu\text{m}$ and $249\text{ }\mu\text{m}$, respectively in the Y-direction; whereas in the X-direction, they were $111\text{ }\mu\text{m}$ and $244\text{ }\mu\text{m}$, respectively. The hole size and repetition were in fair agreement with the $100\text{ }\mu\text{m} \times 100\text{ }\mu\text{m}$ hole and the pitch of $250\text{ }\mu\text{m}$ in the metal mesh. The bias current of 0.16 mA corresponds to 0.8% of the critical current of the meander.

According to a line profile of the transmission image of Fig. 5, we used the sharpness of the dot boundary to estimate a resolution. We found that the resolutions are $22\text{ }\mu\text{m}$ and $41\text{ }\mu\text{m}$ in the Y and X directions, respectively [20]. Higher spatial resolution in the Y direction compared with that in the X direction was consistent with a slower propagation velocity along the Y meanderline compared with that along the X meanderline. We noted that the origin of the error was partially due to the rounding of the etched edges of the holes in the metal mesh. Also, the timestamp determination from the fixed threshold voltage for the analog pulse may involve a timing jitter and result in a pulse-height distribution. We provided a clear demonstration that the delay-line CB-KIDs can be used for energy-dispersive neutron imaging in combination with the Kalliope-DC readout circuit with 1-ns-resolution TDC for the high-speed data acquisition without losing any pulses of the pulsed neutrons from the MLF facility of J-PARC. Clear images of the ^{10}B neutron-absorber dot array were observed, because we avoided the effect of the collimation angle in the neutron beams by placing the test pattern at around 0.8 mm distance from the X/Y CB-KID detectors.

The Kalliope-DC circuit developed for pulsed muons was customized to fit a long frame time of 40 ms at pulsed neutrons of J-PARC so that a time-to-digital converter (TDC) has 32 channels at a sampling clock of 1 ns with a 4 s frame time. Further improvements of the hardware and software of the Kalliope-DC circuit will be fruitful for realizing higher spatial resolution imaging with CB-KID.

To understand the characteristics of the CB-KID fur-

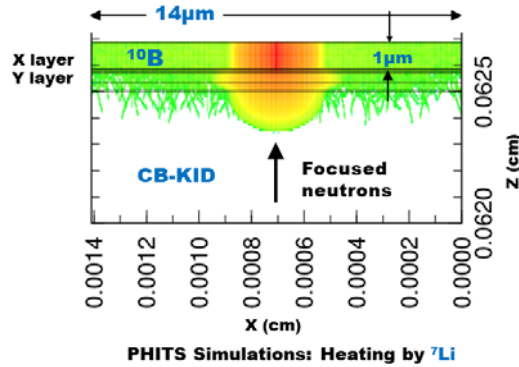


Fig. 6 PHITS simulations of a 14- μm width CB-KID showing local heat dissipation by ${}^7\text{Li}$ particles created by ${}^{10}\text{B}(n,\alpha){}^7\text{Li}$ nuclear reactions in a 1- μm thick ${}^{10}\text{B}$ conversion layer. We used a pencil-type focused neutron beam to demonstrate the usefulness of the PHITS simulations in optimizing the CB-KID design [25].

ther, we performed Monte Carlo simulations using the Particle and Heavy Ion Transport code System (PHITS) [24], [25]. PHITS is able to simulate the physical interactions of various radiations using nuclear reaction models and nuclear data. The simulations model both the trajectories and local energy deposition by neutrons, ${}^7\text{Li}$ particles, ${}^4\text{He}$ particles, electrons, and gamma rays. Figure 6 shows a model of a 14- μm wide section of CB-KID created to understand the local energy dissipation caused by ${}^7\text{Li}$ particles. The energy deposition profile of ${}^4\text{He}$ particles is also similar to Fig. 6, albeit the range of ${}^4\text{He}$ particles is longer than that of ${}^7\text{Li}$ particles by several μm . The PHITS simulations were able to reproduce the neutron transmission image of the simulated ${}^{10}\text{B}$ dot sample. Further improvements in the spatial resolution of CB-KID may be achieved by optimizing the design with the aid of PHITS simulations. It will be worthwhile to investigate the sensitivity of superconducting neutron detectors against other sorts of radiations.

6. Conclusion

The CB-KID neutron detector is remarkable because it can be prepared as one chip on a silicon substrate. This is a main differentiator of CB-KID compared to gas, micro-channel plate, and scintillation detectors. The principle of how signals emerge from CB-KID is completely different to existing detector systems, as it utilizes a local response of the superconducting meanderline. In addition, a delay-line method for imaging the locations of mesoscopic excitations utilizes the long-distance transmission of the electromagnetic signal along the stripline. We confirmed a 52.5-m transmission of the signal using CB-KID, which is not a characteristic of other superconducting detectors. In addition, the CB-KID does not contain any active elements such as single flux quantum (SFQ) devices placed at the cryogenic temperature. This indicates that the CB-KID device is able to use a larger volume for detecting radiations because the space of the substrate for installing active devices can be saved. We expect that the 10 mm \times 10 mm sensitive area

of the CB-KID device will be able to achieve mega-pixel imaging using only the four readouts. Since the physical process of signal generation and propagation can proceed on a sub-millimeter regime, the whole dimension of a CB-KID chip can be built with a thickness of less than a few millimeters. Other neutron detectors need an optical light path, gas-amplification, a Complementary Metal Oxide Semiconductor Image Sensor (CMOS) or a Charge-Coupled Device (CCD) for imaging. The CB-KID does not need such devices, which require extra space. In addition, CB-KID has a ${}^{10}\text{B}$ neutron-conversion layer, while the rest of the detector is basically transparent to neutron beams. This makes it possible to assemble several CB-KIDs in a stacked configuration when neutron imaging. This is particular to the CB-KID while other detectors cannot be stacked as they need extra space for parts other than the detector as mentioned above.

The current development status of CB-KID is not the ultimate state, and further improvements can be expected in the future. Achieving the goal of sub-micrometer resolution neutron imaging requires (1) improvement of the temporal resolution of a time-to-digital converter (TDC) to overcome the limit of the line-and-space pitch of the superconducting meanderline, (2) compensation of the random emitting directions of the charged particles (${}^4\text{He}$, ${}^7\text{Li}$) from the nuclear reaction ${}^{10}\text{B}(n,\alpha){}^7\text{Li}$, (3) enhancement of the spatial resolution by data processing of multiply-stacked CB-KIDs, (4) development of fabrication technique to fulfill a sub-micrometer line and spacing of the Nb meanderline with no disconnections, and (5) exploration of the possibility of using a ${}^3\text{He}$ refrigerator to cool down the CB-KID to ensure a narrower signal pulses by suppressing dissipation caused by quasiparticles. We wish that further improvements of the CB-KID devices are explored in a coordinated manner using high-end neutron facilities. The main interest is to enhance the neutron flux density in the coming future.

Acknowledgments

This work was conducted in collaboration with K. Takahashi, D. Fujiwara, M. Nishikawa, Y. Fujita, K. Arai, Y. Akita, I. Yagi, Y. Kodama, N. Yoshioka, Y. Narukami, A. Nomura, H. Yamaguchi, H. Nakayama, Y. Miki, Y. Iizawa, K. Nishimura, S. Miki, A. Saito, H. Shimakage, A. Kawakami, Z. Wang, K. Sato, M. Uno, T. Yotsuya, K. Moriwaki, H. Fukuda, F. Kusunoki, M. Kato, S. Okayasu, K. Hojo, M. Katagiri, Y. Morii, N. Niimura, K. Soyama, K. Aizawa, K. Oikawa, M. Harada, T. Oku, M. Arai, T. Shinohara, M. Machida, T. Kano, A. Malins, A. Fujimaki, M. Hidaka, S. Miyajima, H. Shishido, T.D. Vu, T. Koyama, K.M. Kojima, S. Suzuki, and M.M. Tanaka. The author benefitted from stimulating discussions with J. Akimitsu, H. Fukuyama, K. Kitazawa, Y. Fujii, H. Yasuoka, and M. Motokawa.

This work was partially supported by Grants-in-Aid for Scientific Research (Grant Nos. JP16360477, JP16H02450, JP19206104, JP23246173, JP23226019,

JP16H02450) from JSPS and by CREST. The neutron-irradiation experiments at the Materials and Life Science Experimental Facility (MLF) of the J-PARC were conducted under the support of MLF programs (Proposals Nos. 2015A0129, 2016B0112, 2017A0011, 2017B0014, 2018A0109, 2015P0301, 2016P0301, 2018P0201).

References

- [1] M. Kurakado and H. Mazaki, "Quasiparticle excitation in a superconducting tunnel junction by α particles," *Phys. Rev. B*, vol.22, no.1, pp.168–173, 1980.
- [2] M. Kurakado and H. Mazaki, "Possibility of a high-resolution nuclear radiation detector using a superconductor: I. Mean energy loss per excess quasiparticle," *Nucl. Instr. Meth.*, vol.185, no.1-3, pp.141–147, 1981.
- [3] M. Kurakado and H. Mazaki, "Possibility of a high-resolution nuclear radiation detector using a superconductor: II. Tunnel junction," *Nucl. Instr. Meth.*, vol.185, no.1-3, pp.149–155, 1981.
- [4] K.D. Irwin, G.C. Hilton, D.A. Wollman, and J.M. Martinis, "X-ray detection using a superconducting transition-edge sensor microcalorimeter with electrothermal feedback," *Appl. Phys. Lett.*, vol.69, no.13, pp.1945–1947, 1996.
- [5] J.A. Chervenak, K.D. Irwin, E.N. Grossman, J.M. Martinis, C.D. Reintsema, and M.E. Huber, "Superconducting multiplexer for arrays of transition edge sensors," *Appl. Phys. Lett.*, vol.74, no.26, pp.4043–4045, 1999.
- [6] G.N. Gol'tsman, O. Okunev, G. Chulkova, A. Lipatov, A. Semenov, K. Smirnov, B. Voronov, A. Dzardanov, C. Williams, and R. Sobolewski, "Picosecond superconducting single-photon optical detector," *Appl. Phys. Lett.*, vol.79, no.6, pp.705–707, 2001.
- [7] S. Miki, T. Yamashita, M. Fujiwara, M. Sasaki, and Z. Wang, "Multichannel SNSPD system with high detection efficiency at telecommunication wavelength," *Optics Letters*, vol.35, no.13, pp.2133–2135, 2010.
- [8] B.A. Mazin, P.K. Day, J. Zmuidzinas, and H.G. Leduc, "Multiplexable kinetic inductance detectors," *AIP Conf. Proc.*, vol.605, no.1, pp.309–312, 2002.
- [9] K. Hashimoto, K. Ohya, and Y. Yamane, "Dead-Time Measurement for Radiation Counters by Variance-to-Mean Method," *J. Nucl. Sci. Tech.*, vol.33, no.11, pp.863–868, 1996.
- [10] D.S. Hussey, J.M. LaManna, E. Baltic, and D.L. Jacobson, "Neutron imaging detector with $2\ \mu\text{m}$ spatial resolution based on event reconstruction of neutron capture in gadolinium oxysulfide scintillators," *Nucl. Instrum. Meth. Phys. Res. A*, vol.866, pp.9–12, 2017.
- [11] A.S. Tremsin, J. Rakovan, T. Shinohara, W. Kockelmann, A.S. Losko, and S.C. Vogel, "Non-destructive study of bulk crystallinity and elemental composition of natural gold single crystal samples by energy-resolved neutron imaging," *Sci. Rep.*, vol.7, p.40759-1-9, 2017.
- [12] J. Nagamatsu, N. Nakagawa, T. Muranaka, Y. Zenitani, and J. Akimitsu, "Superconductivity at 39 K in magnesium diboride," *Nature*, vol.410, no.6824, pp.63–64, 2001.
- [13] K. Takahashi, K. Satoh, T. Yotsuya, S. Okayasu, K. Hojou, M. Katagiri, A. Saito, A. Kawakami, H. Shimakage, Z. Wang, and T. Ishida, "Design of neutron detector by using a novel superconductor MgB_2 ," *Physica C*, vol.392-396, part 2, pp.1501–1503, 2003.
- [14] T. Ishida, M. Nishikawa, Y. Fujita, S. Okayasu, M. Katagiri, K. Satoh, T. Yotsuya, H. Shimakage, S. Miki, Z. Wang, M. Machida, T. Kano, and M. Kato., "Superconducting MgB_2 Thin Film Detector for Neutrons," *J. Low Temp. Phys.*, vol.151, no.3-4, pp.1074–1079, 2008.
- [15] H. Shibata, "Fabrication of a MgB_2 nanowire single-photon detector using $\text{Br}_2\text{-N}_2$ dry etching," *Appl. Phys. Express*, vol.7, no.10, p.103101-(1-4), 2014.
- [16] H. Shishido, T. Yoshida, and T. Ishida, "Ambient temperature epitaxial growth of MgB_2 thin films with a Mg buffer layer," *Appl. Phys. Express*, vol.8, no.11, p.113101-(1-3), 2015.
- [17] S. Miyajima, H. Shishido, Y. Narukami, N. Yoshioka, A. Fujimaki, M. Hidaka, K. Oikawa, M. Harada, T. Oku, M. Arai, and T. Ishida, "Neutron flux spectrum revealed by Nb-based current-biased kinetic inductance detector with a ^{10}B conversion layer," *Nucl. Instr. Meth. Phys. Res. A*, vol.842, pp.71–75, 2017.
- [18] Y. Narukami, S. Miyajima, A. Fujimaki, M. Hidaka, and T. Ishida, "20 ps Pulsed Laser Irradiation to Current-Biased Kinetic Inductance Detector Made of Nb Nanowires," *IEEE Trans. Appl. Supercond.*, vol.25, no.3, p.2400904-(1-4), 2015.
- [19] H. Shishido, S. Miyajima, Y. Narukami, K. Oikawa, M. Harada, T. Oku, M. Arai, M. Hidaka, A. Fujimaki, and T. Ishida, "Neutron detection using a current biased kinetic inductance detector," *Appl. Phys. Lett.*, vol.107, no.23, p.232601-(1-4), 2015.
- [20] H. Shishido, Y. Miki, H. Yamaguchi, Y. Iizawa, V.T. Dang, K.M. Kojima, T. Koyama, K. Oikawa, M. Harada, S. Miyajima, M. Hidaka, T. Oku, K. Soyama, S.Y. Suzuki, and T. Ishida, "High-Speed Neutron Imaging Using a Current-Biased Delay-Line Detector of Kinetic Inductance," *Phys. Rev. Applied*, vol.10, no.4, p.044044-(1-10), 2018.
- [21] T. Koyama and T. Ishida, "Electrodynamics theory for the operation principle of a superconducting kinetic inductance stripline detector," *J. Phys. Conf. Ser.*, vol.1054, no.1, p.012055-(1-8), 2018.
- [22] T. Koyama and T. Ishida, "Ginzburg-Landau theory for the operation principle of superconducting delay-line inductance detectors," *J. Phys. Conf. Ser.*, vol.1293, p.012050-(1-8), 2019.
- [23] S. Miyajima, H. Yamaguchi, H. Nakayama, H. Shishido, A. Fujimaki, M. Hidaka, M. Harada, K. Oikawa, T. Oku, M. Arai, and T. Ishida, "Development of a neutron imager based on superconducting detectors," *Physica C: Superconductivity and its applications*, vol.530, pp.98–100, 2016.
- [24] T. Sato, Y. Iwamoto, S. Hashimoto, T. Ogawa, T. Furuta, S. Abe, T. Kai, P.-E. Tsai, N. Matsuda, H. Iwase, N. Shigyo, L. Silver, and K. Niita, "Features of Particle and Heavy Ion Transport code System (PHITS) version 3.02," *J. Nucl. Sci. Tech.*, vol.55, no.6, pp.684–690, 2018.
- [25] A. Malins, M. Machida, T.D. Vu, K. Aizawa, and T. Ishida, "Monte Carlo Radiation Transport Modelling of the Current-Biased Kinetic Inductance Detector," *Nucl. Instr. Meth. Phys. Res. A*, vol.953, p.163130-(1-7), 2020.



Takekazu Ishida received his B.E. from Tohoku University, Sendai, Japan, in 1976. He received M.E. and Ph.D. degrees from Kyoto University in 1978 and 1982, respectively. He has been working on material properties of superconductors for years and developed instruments using nonlinear magnetic susceptibility, magnetic torque, and a scanning SQUID microscope. He proposed the idea to make a neutron detector using an MgB_2 superconductor and a current-biased kinetic inductance detector in a

delay-line operation. His research interests are the fundamental properties of superconductors and applications of superconducting devices. He was a professor in the Department of Physics and Electronics at Osaka Prefecture University until March 2018. In April 2018 he became a guest professor in the Division of Quantum and Radiations Engineering at Osaka Prefecture University. He is a member of the Physical Society of Japan, the American Physical Society, and the Cryogenics and Superconductivity Society of Japan.